

Lithological and structural controls on river profiles and networks in the northern Sierra Nevada (California, USA)

Emmanuel J. Gabet[†]

Department of Geology, San Jose State University, San Jose, California 95192, USA

ABSTRACT

In this study, the strong lithological heterogeneity of the northern Sierra Nevada (California, USA) is exploited to elucidate the role of lithology on river profiles and patterns at the mountain-range scale. The analyses indicate that plutonic, metavolcanic, and quartzite bedrock generally host the steepest river reaches, whereas gentle reaches flow across non-quartzite metasedimentary rocks and fault zones. In addition, the largest immobile boulders are often in the steepest reaches, suggesting that wide joint spacing plays a role in creating steep channels, and a positive relationship between boulder size and hillslope angle highlights the coupling of the hillslope and fluvial systems. With respect to river network configurations, dendritic patterns dominate in the plutonic bedrock, with channels aligned down the slope of the range; in contrast, river reaches in the metamorphic belts are mainly longitudinal and parallel to the structural grain. River profiles and patterns in the northern Sierra Nevada, therefore, bear a strong lithological imprint related to differential erosion. These observations indicate that attempts to infer uplift and tilting of the range based on the gradients and orientations of paleochannel remnants should first account for the effect of bedrock erodibility. Indeed, the differences in gradients of Tertiary paleochannel remnants used to argue for late Cenozoic uplift of the range can be wholly explained by differences in lithology.

INTRODUCTION

The longitudinal profile of a river is often idealized as a smooth concave form, with steep reaches in the headwaters gradually transitioning to gentler reaches as the channel loses elevation (e.g., Inoue, 1992; Larue, 2008). In the upper reaches, where channels incise into bedrock,

deviations from this shape can be attributed to a variety of causes, such as changes in lithology along the river's course (e.g., Duvall et al., 2004; Lecce, 1997; Phillips and Lutz, 2008; Pike et al., 2010), spatial variations in the delivery of coarse sediment to the channel (e.g., Finnegan et al., 2017; Hack, 1973; Hanks and Webb, 2006), and drainage capture (Fan et al., 2018). River profiles may also be modified by crustal deformation, thereby offering the potential for obtaining information about tectonic activity that might otherwise be difficult to acquire (e.g., Pavano et al., 2016).

However, before river profiles can be reliably used for inferring tectonic activity, other factors that can affect their shape must first be considered. Although important advances have been made, the development of mechanistic theories for describing the incision processes that determine a bedrock river's profile is still ongoing (e.g., Chatanantavet and Parker, 2009; Lamb et al., 2015; Sklar and Dietrich, 2006b; Whipple et al., 2000). Indeed, our understanding of the controls on bedrock channel gradients is incomplete and predicting how steep a reach should be, even given complete information regarding discharge, underlying lithology, sediment supply, and tectonic history, remains challenging.

This study presents a large-scale analysis of the influence of lithology and structure on river profiles and network configurations along the western slope of the northern Sierra Nevada (California, USA) (Fig. 1). Because of its history as a subduction zone during the Jurassic and Cretaceous periods, this region is lithologically complex (e.g., Snow and Scherer, 2006). From the western margin of the range to its eastern ridgeline, the pre-Cenozoic basement generally consists of north-south-trending belts of Mesozoic metasedimentary and metavolcanic rocks, parallel belts of Paleozoic metasedimentary and metavolcanic units, and, finally, plutonic rocks (albeit with some isolated remnants of Mesozoic metamorphic rocks) underlying the crest (Saucedo and Wagner, 1992; Wagner et al., 1981). Although plutonic rocks dominate the eastern half of the range, there are

numerous smaller plutonic intrusions throughout the metamorphic belts. Because the belts of metamorphic rocks, separated by fault zones, are aligned parallel to the ridge-crest, rivers flowing down the western slope of the range encounter a variety of rock types with differing erodibilities; this region, therefore, provides an opportunity for examining the role of spatially varying bedrock on river profiles and planforms. Moreover, an analysis of the modern rivers is critical for assessing the results of studies that have used the profiles of Sierran paleochannels to infer late Cenozoic uplift of the range (Hudson, 1955; Jones et al., 2004; Lindgren, 1911; Yeend, 1974).

MATERIALS AND METHODS

Longitudinal Profiles and Slope Calculations

This study focuses on five major river systems draining the northern Sierra Nevada (Fig. 1). The headwaters of many of these rivers are located on a relatively low-relief bedrock surface that dominates much of the high-altitude terrain in the region; from this low-relief surface, the rivers cascade down into deep canyons with steep slopes. The longitudinal profiles of five trunk streams (Fig. 1) were extracted from 30 m digital elevation models (DEMs) in a geographical information system (GIS) using standard techniques (O'Callaghan and Mark, 1984). The upper extents of the South Yuba River, the South Fork American River, and the North Fork Mokelumne River profiles were established where the drainage area exceeds ~100 km² to avoid, as much as possible, sections where these channels flow across the low-relief bedrock surface and have failed to incise into it to an appreciable degree. The upper extent of the North Fork Feather River profile was established downstream of a region of faults active in the Quaternary (Saucedo and Wagner, 1992), and the upper extent of the Merced River was established downstream of the alluviated Yosemite Valley. The downstream extent of each profile

[†]manny.gabet@sjsu.edu

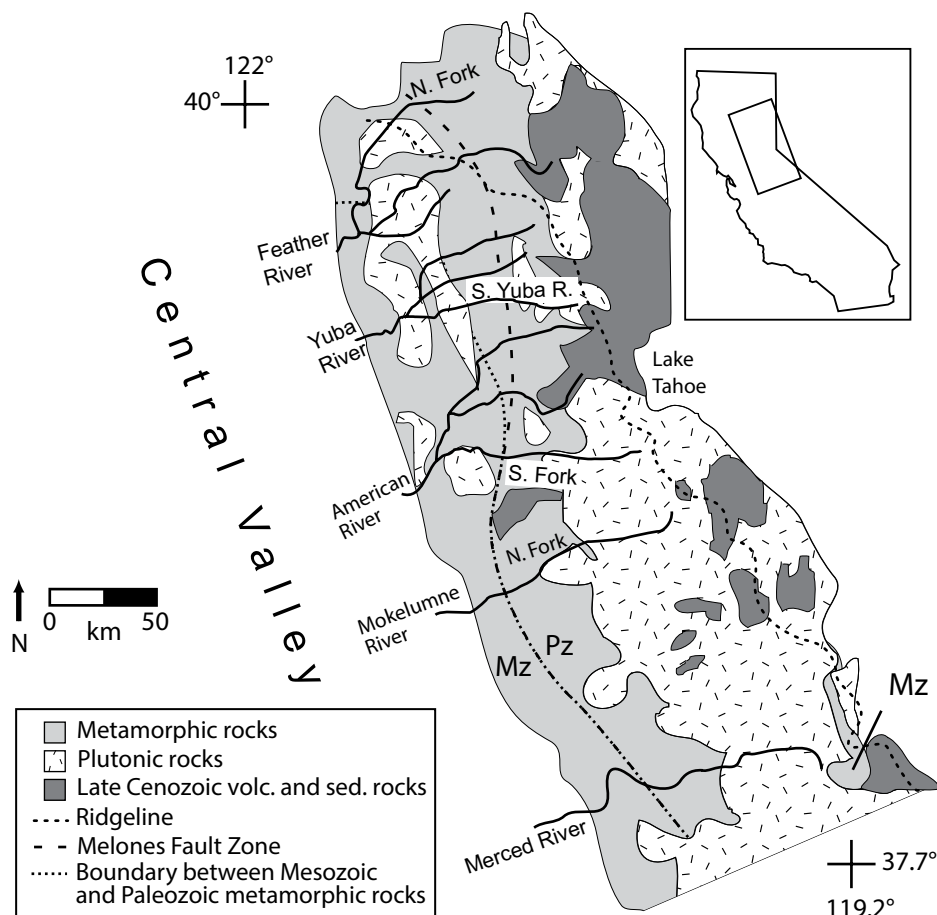


Figure 1. Generalized lithological map of study area (Sierra Nevada, California, USA). Labeled rivers were analyzed in this study. Modified from Parrish (2006). N.—North; S.—South; R.—River; Mz—Mesozoic; Pz—Paleozoic; volc.—volcanic; sed.—sedimentary.

was terminated where it meets one of the large reservoirs built along the Sierran foothills.

The elevations of lithological boundaries along each channel profile were determined from paper maps (Bateman and Krauskopf, 1987; Hietanen, 1973; Peck, 2002; Saucedo and Wagner, 1992; Wagner et al., 1991; Wagner et al., 1981) and a GIS layer (Ludington et al., 2005). The different sources were used to cross-check the precise locations of the boundaries.

The average channel slope across each lithological unit was calculated from the difference in elevation of the reach, from one lithological boundary to the next, and the length of the reach (note, the term “reach” is used throughout to describe a section of river flowing across a single lithological unit). To account for the tendency of river gradients to decrease with increasing drainage area (Hack, 1957), the steepness index (k_s), which normalizes river gradient (S) according to drainage area (A), was calculated with

$$k_s = A^\theta S, \quad (1)$$

where θ is the concavity of a channel’s profile (Flint, 1974). By determining a common concavity between watersheds (i.e., a reference concavity, θ_{ref}), values of k_s for individual reaches of different rivers can be compared (Wobus et al., 2006). A reference concavity of 0.35 for the study area was calculated by analyzing the longitudinal profiles of tributary watersheds (Supplemental Information, Fig. DR1¹) using the chi analysis algorithm in LSDTopoTools (Mudd et al., 2014; Mudd et al., 2018a; Mudd et al., 2018b; Perron and Royden, 2013). The use of Equation (1) to provide a steepness index is not meant to imply that the region is in topographic steady-state (see later). This approach is adopted because it facilitates comparisons of the gradients of individual reaches, but it is not used to investigate the overall profiles of the channels.

¹GSA Data Repository item 2019274, calculations of reference concavity and peak discharges, is available at <http://www.geosociety.org/datarepository/2019> or by request to editing@geosociety.org.

Finally, note that the upper sections of three of the rivers studied here (the South Yuba, the North Fork of the Mokelumne, and the Merced rivers) were occupied by glaciers during the Pleistocene ice ages (Gillespie and Clark, 2011). However, as with other glaciated canyons in the Sierra Nevada (Brocklehurst and Whipple, 2002; Dühnforth et al., 2010; Matthes, 1930; Zimmer and Gabet, 2018), vertical incision by the glaciers appears to have been limited (Bateman and Wahrhaftig, 1966), and there is no evidence that the longitudinal profiles of these valleys were substantially affected. In any case, since both rivers and glaciers incise via plucking and abrasion, differences in rock erodibility ought to be similarly reflected in the profiles they create.

Channel and Valley Characteristics

Lithological differences may not only be expressed in channel slopes but also in channel widths and the size of the bed sediment (e.g., Duvall et al., 2004; Montgomery and Gran, 2001). Moreover, in mountainous terrain where the valleys are narrow, the fluvial system is tightly coupled to the adjacent hillslopes; fluvial processes, therefore, may be influenced by the surrounding terrain. These additional factors were examined along a subset of the studied channels. Because reaches along these rivers are typically inaccessible due to steep terrain, bankfull channel width was measured at ~500 m intervals from high-resolution (0.5 m) Google Earth imagery using the ruler tool along the North Fork of the Feather River, the South Yuba River, and the Merced River. These three were chosen because, of the five investigated here, their lithology has been mapped in the greatest detail and the available Google Earth imagery for these sites is of high quality (e.g., the water is at low flow and clear, there are few shadows due to a high sun angle, etc.). The photographs were taken during low-flow conditions in the summer of 2017, therefore visual cues, including vegetation lines and color differences along the banks, were used to estimate bankfull conditions. Record rainfall during the winter and spring of 2016–2017 (Lin and St. John, 2017), before the photographs were taken, led to high discharges that left behind clear trimlines along most of the reaches. Moreover, the V-shaped cross-section of many of the valleys implies that channel width increases slowly with discharge, thus constraining errors in these measurements. Nevertheless, I estimate an uncertainty of ± 10 m in the measurement of the bankfull channel widths.

The long axis of the largest boulder within a radius of ~25 m around each channel-width-measurement site was also estimated with the

ruler tool in Google Earth for the three aforementioned rivers and along an anomalous section of the North Fork Mokelumne River. Because of the low-flow conditions in the images and the clarity of the water, large boulders can be easily seen in the imagery. However, for clasts smaller than 0.5 m, a default value of 0.5 m was assigned. The maximum uncertainty in these measurements is likely on the order of ± 2 m for the largest boulders, primarily because the lower parts of these clasts were submerged and their outlines sometimes difficult to identify precisely.

Google Earth does not provide information regarding its orthorectification procedures; this issue, as well as others regarding Google Earth imagery (Fisher et al., 2012), suggests that some measurements could be incorrect because of photographic distortion. To gauge the potential for measurement error, orthorectified aerial photographs from the National Agricultural Imagery Program (NAIP, 2018) for a subsample of the sites were imported into a GIS. The dimensions of stable features such as large boulders and roads were measured from both the NAIP (0.5 m resolution; Fisher et al., 2012) and Google Earth imagery and compared. The average difference in measurements between both sets of photographs was 0.2 ± 0.2 m ($n = 20$), indicating minimal errors due to photographic distortion.

Valley relief along each channel was calculated from the 30 m DEMs by subtracting the river elevation from the highest elevation found within a 1000 m radius, a distance sufficient to include the valley rims. The mean angle of the hillslopes along each river was determined by averaging the slopes of all cells with slopes $> 15^\circ$ within a 240 m radius of each river cell; cells with slopes $\leq 15^\circ$ were excluded to avoid floodplains, terraces, and fans. The radius was chosen to avoid terrain above the canyon rims.

Shear Stress Calculations

A river's boundary shear stress (τ_b) plays an important role in controlling the rates of channel incision (e.g., Lamb et al., 2015). For the three rivers where boulder size and channel width were measured along their entire study length, reach-averaged maximum shear stresses were estimated with

$$\tau_b = \gamma Q^{0.6} n^{0.6} S^{0.7} w^{-0.6}, \quad (2)$$

where γ is the unit weight of water, Q is discharge, n is Manning's roughness coefficient, S is the reach-averaged slope, and w is the reach-averaged channel width (Snyder et al., 2003). For each reach, Q was estimated from the contributing area based on discharge records during the January 1997 floods in the northern Sierra Ne-

vada (Supplemental Information; see footnote 1). Manning's n was estimated with $n = 0.034 D_{90}^{1/6}$ where D_{90} , the ninetieth percentile of the particle size distribution, was approximated by reach-averaged values of the maximum boulder size (USACE, 1994); although this approach likely overestimated the roughness coefficient and, thus the shear stress, the error is tempered somewhat by the low value of the exponent.

River Network Analysis

To investigate the role of lithology and structure in controlling the shape of the river networks, all the channels within the study region were extracted from a 30 m DEM using an accumulation area threshold of 10 km². The channels were split into ~ 5 km sections, and the azimuth of each section was calculated in ARCGIS using the EasyCalculate 10 add-in (www.ian-ko.com/free/EC10/EC10_main.htm). In addition, the bedrock underlying each section was extracted from a digital lithological map of California (Ludington et al., 2005). Channel sections in metamorphic bedrock east of the Melones Fault Zone (Fig. 1) were excluded from the analyses because of the dominance of a subduction mélange (the Paleozoic Calaveras Complex) in which the various lithological units have been jumbled together (Snow and Scherer, 2006).

RESULTS

River Gradient and Lithology

The results from the profile analyses are presented from north to south. Along the North Fork Feather River (henceforth referred to as the NF Feather River), all of the breaks-in-slope are found at or near lithological contacts (although not every contact produces a break-in-slope), and the gradients of individual reaches often vary according to lithology (Fig. 2). The reaches with the steepest median k_s are underlain by metavolcanic rocks (0.23 ± 0.04 ; Table 1), followed by reaches flowing over plutonic rocks (0.15 ± 0.02) and non-quartzite metasedimentary bedrock (0.02). Interestingly, within the plutonic rocks, the difference in gradients can be substantial. For example, the slope across the lower exposure of the quartz diorite (KJhq) at km-19) is $\sim 3\times$ times steeper than the reach across the pyroxene diorite just upstream (KJpd at km-15). The gentlest reach is across a fault zone (ultramafic/metavolcanic at km-52); where the river crosses similar bedrock upstream (ultramafic/metavolcanic/metasedimentary at km-40), the gradient is $3\times$ times higher.

Along the South Yuba River (Fig. 3A), the plutonic and quartzite rocks have the highest

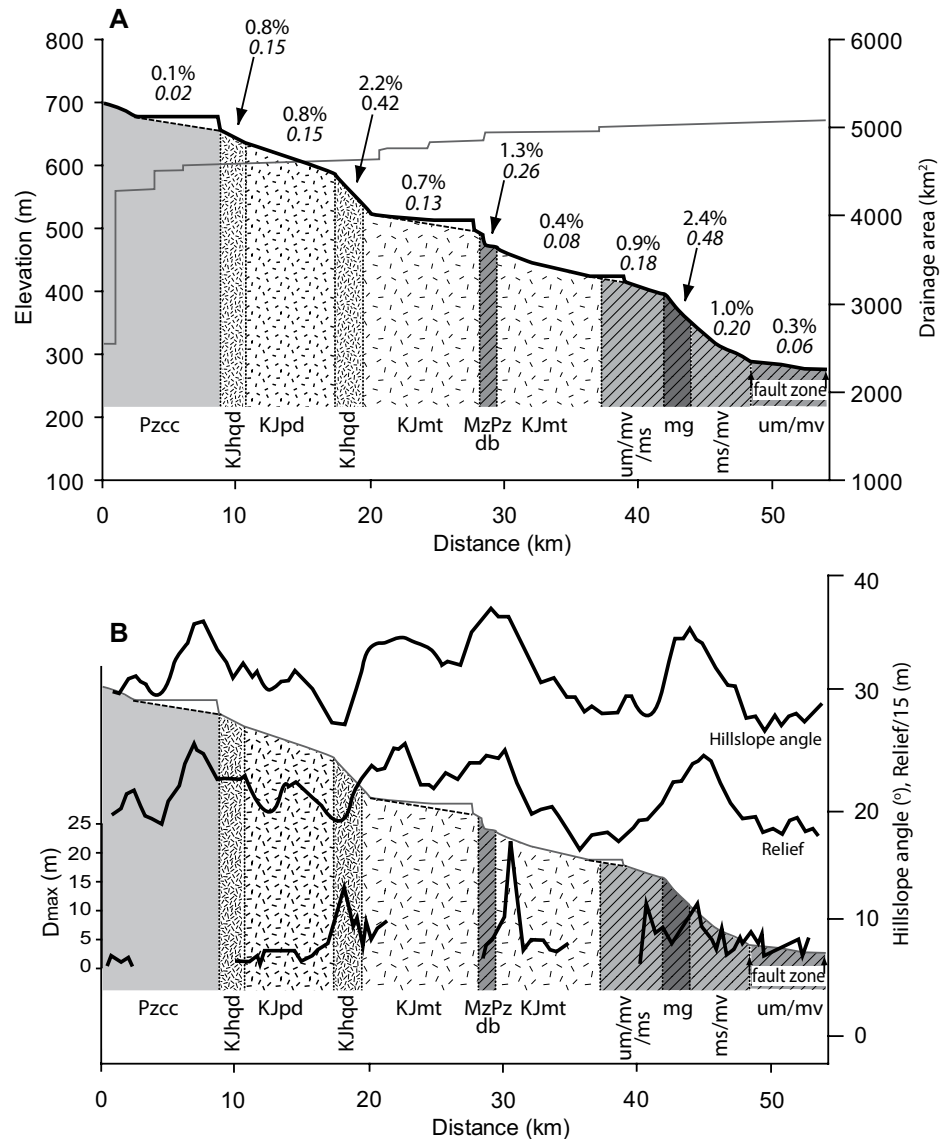
median k_s , 0.20 ± 0.06 and 0.20 ± 0.07 , respectively (Table 1). In contrast to the NF Feather River, the unfaulted metavolcanic bedrock has a low k_s (0.08), similar to the non-quartzite metasedimentary rocks (0.09 ± 0.01). Where the river crosses the fault zone near km-80, the profile abruptly flattens. The overall profile of the South Yuba River is stair-stepped, with steep reaches over plutonic rock connected to gently-sloping reaches across fault zones and non-quartzite metasedimentary rock.

The profile of the South Fork American River (henceforth referred to as the SF American River) also has breaks-in-slope associated with lithological contacts (Fig. 4). This trend is particularly apparent in the section of river from km-32 to km-72, where steep reaches across granitic rocks (median $k_s = 0.16 \pm 0.09$; Table 1) are juxtaposed with gentle reaches across mainly non-quartzite metasedimentary rocks (median $k_s = 0.10 \pm 0.01$). There are exceptions, however, to this general pattern; for example, in the section of river between km-20 and km-34, a plutonic unit has slopes comparable to its non-quartzite metasedimentary neighbors. Similarly, the reach of river flowing over granitic bedrock at km-80–90 has nearly the same k_s as the adjoining downstream reach flowing across non-quartzite metasedimentary rocks. Finally, note the significant break-in-slope in the upper reaches of the SF American River (km-8). Mapping of the plutonic rocks in this watershed has not been as detailed as in others, and the bedrock has only been generically identified as Mesozoic granite (Wagner et al., 1981); this break-in-slope, therefore, may be associated with an unmapped inter-plutonic contact (compare with km-10–28 on the NF Feather River; Fig. 2A).

Along the North Fork Mokelumne River (henceforth referred to as the NF Mokelumne River), the reaches flowing over the plutonic rocks are generally steeper (median $k_s = 0.17 \pm 0.08$; Table 1) than those over the non-quartzite metasedimentary rocks (0.09 ± 0.04). A notable feature of this river is the cascade (km-65–70) straddling the lithological contact between granitic rocks (Mzg; Fig. 5) and the metasedimentary rocks of the Calaveras Complex (Pzcc). The metasedimentary bedrock has been deeply incised relative to the granitic rocks just upstream to form a ~ 200 -m-high knickpoint. At the base of the knickpoint, a large tributary increases the drainage area by 40%, and the abrupt increase in flow may be partially responsible for the deeper incision through the weaker rock.

Of the five rivers analyzed in this study, the reaches of the Merced River (Fig. 6A) have the greatest difference in median k_s between the plutonic rocks (0.40 ± 0.05) and the non-quartzite metasedimentary bedrock (0.08 ± 0.02). This

Figure 2. (A, B) Longitudinal profile, lithology, and other data along the North Fork Feather River (adapted from Johnson, 2015). Gradient and k_s (steepness index; in italics) shown above each reach. Plutonic rocks designated by patterned fills; metavolcanic rocks designated by hatch pattern; metasedimentary rocks designated by solid shading. Pzcc—metachert, argillite; KJhqd—coarse-grained quartz diorite; KJpd—fine- to medium-grained pyroxene diorite; KJmt—coarse-grained monzotonalite; MzPz db—metabasalt; um—ultramafic; mv—metavolcanic; mg—metagabbro; ms—metasedimentary; the four rock types at the end of the profile are of Mesozoic and Paleozoic ages (Hietanen, 1973; Saucedo and Wagner, 1992). Fill patterns represent the distribution of bedrock units at the surface and not the underlying structure. Gaps in D_{\max} (maximum particle size) are due to reservoirs.



sharp difference is perhaps attributable to the segregation of the different rock types into zones that are more distinct than along the other four channels. The quartzite bedrock has a k_s value of 0.17, intermediate between the other two rock types. The differences in gradients between the different plutonic bedrocks are modest, and the two main breaks-in-slope in the profile are within individual reaches rather than at their boundaries. The first, at km-2, leads into a relatively flat section where the river follows a master joint, and the second, at km-11, is discussed later.

Channel and Hillslope Characteristics

No relationship between channel widths and lithology could be detected (Fig. 7). The maximum particle size (D_{\max}), however, appears to be controlled by lithology whereby, in general, $D_{\max\text{-plut.}} > D_{\max\text{-metavol.}} > D_{\max\text{-qtzt}} > D_{\max\text{-metased.}}$ (Table 2). Considering that many of the boulders are angular and quite large, they likely have not experienced much fluvial transport; indeed, estimated shear stresses during one of the largest floods on record were 10x lower than the critical shear stresses (Fig. 8). The spatial distribution of D_{\max} , therefore, should reflect the delivery of sediment from the adjacent slopes (Hack, 1957). Indeed, D_{\max} is positively correlated with average hillslope angle in plutonic and metavolcanic terrain (Fig. 9). A similar relationship could not be detected in the metasedimentary rocks, perhaps because this rock type sometimes produces clast sizes below the limit of resolution (i.e., smaller than 0.5 m). Within the plutonic rocks,

joint density appears to play an important role in the maximum size of boulders entering the rivers. For example, on the NF Feather River, the source of the 22 m boulder at km-31 is a set of large, unjointed exfoliation sheets forming a cliff above the channel (note the steep hillslopes

at this site; Fig. 2B). Similarly, at km-18, there is an abrupt 3-fold increase in D_{\max} from one plutonic rock to the next, presumably a consequence of joint spacing. A peak in boulder size is also coincident with a steep reach along the South Yuba River at km-22–28 (Fig. 3B).

TABLE 1. MEDIAN k_s AND MEDIAN ABSOLUTE DEVIATION ACCORDING TO ROCK TYPE

| | Plutonic | Metavolcanic | Quartzite | Non-quartzite metasedimentary |
|---------------------|------------------|-----------------|-----------------|-------------------------------|
| NF Feather River | 0.15 ± 0.02 (5) | 0.23 ± 0.04 (4) | N.D. | 0.02 (1) |
| South Yuba River* | 0.20 ± 0.06 (7) | 0.08 (1) | 0.20 ± 0.07 (2) | 0.09 ± 0.01 (2) |
| SF American River | 0.16 ± 0.09 (6) | 0.05† (1) | N.D. | 0.10 ± 0.01 (6) |
| NF Mokelumne River§ | 0.17 ± 0.08 (7) | N.D. | N.D. | 0.09 ± 0.04 (5) |
| Merced River | 0.40 ± 0.05 (5) | N.D. | 0.17 (1) | 0.08 ± 0.02 (2) |
| All rivers | 0.17 ± 0.07 (30) | 0.19 ± 0.09 (6) | 0.17 ± 0.04 (3) | 0.09 ± 0.02 (16) |

Note: Rock units in fault zones were excluded. Sample sizes in parentheses. N.D.—no data; SF—South Fork; NF—North Fork; k_s —steepness index.

*Only reaches after km-20 were included to avoid the low-relief region where fluvial incision appears insignificant.

†Highly sheared mélangé terrane (Wagner et al., 1981).

§Reaches at km-60 and km-70 (Fig. 5) were split because of the large differences in gradients within the individual units.

Figure 3. (A, B) Longitudinal profile, lithology, and other data along the South Yuba River. Gradient and k_s (steepness index; in italics) shown above each reach. Plutonic rocks designated by patterned fills; metavolcanic rocks designated by hatch pattern; metasedimentary rocks designated by solid shading. KJgr—granite, granodiorite; Jms—metasedimentary; Jmv—metavolcanic; Jdi—diorite; Pzsf ss—quartzite, phyllite; Dbg—granite, granodiorite; Pzp—peridotite; Pzcc—metachert, argillite; Pzcv—metavolcanic; MzPz ms—metasedimentary; Jgr—granite, granodiorite; gb—gabbro, diabase; um—ultramafic; mv—metavolcanic; qd—metadiorite; the three rock types at the end of the profile are of Mesozoic and Paleozoic ages (Hietanen, 1973; Saucedo and Wagner, 1992). Fill patterns represent the distribution of bedrock units at the surface and not the underlying structure. Data gaps are due to a large reservoir. “LGM” points to glacial extent during the last glacial maximum. D_{\max} —maximum particle size.

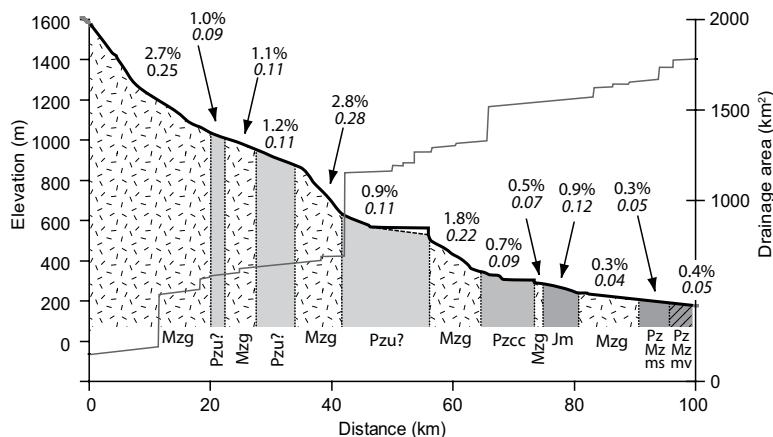
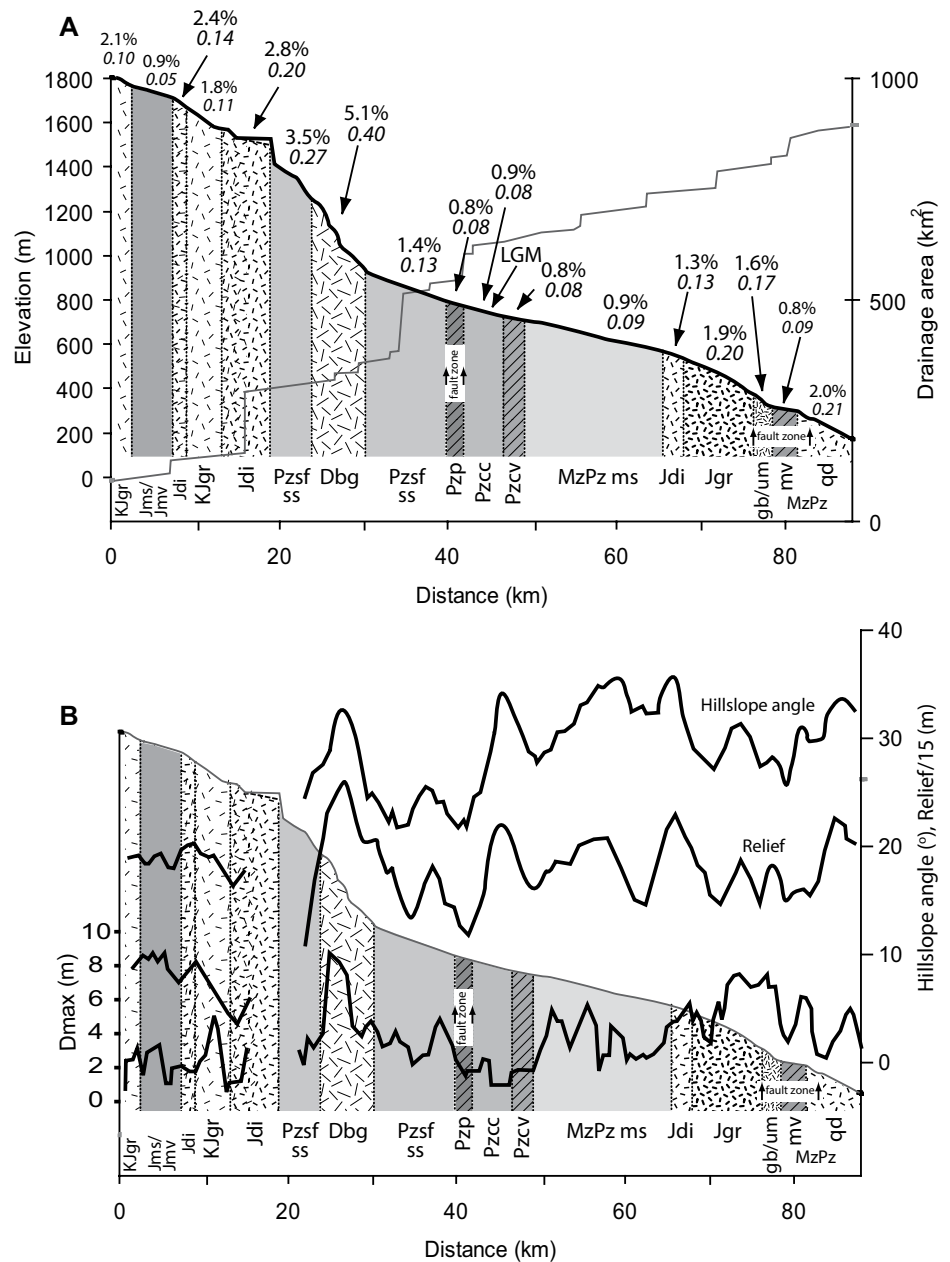


Figure 4. Longitudinal profile and lithology along the South Fork American River. Gradient and k_s (steepness index; in italics) shown above each reach. Plutonic rocks designated by patterned fills; metavolcanic rocks designated by hatch pattern; metasedimentary rocks designated by solid shading. Mzg—granitic; Pzu?—undifferentiated; Pzcc—metachert, argillite; Jm—slate, greywacke, conglomerate; ms—metasedimentary (mélange terrane); mv—metavolcanic (mélange terrane) (Wagner et al., 1981). Fill patterns represent the distribution of bedrock units at the surface and not the underlying structure.

Figure 5. Longitudinal profile and lithology along the North Fork Mokelumne River. Gradient and k_s (steepness index; in *italics*) shown above each reach. Plutonic rocks designated by patterned fills; metasedimentary rocks designated by solid shading. Mzg—granitic; Mzd—dioritic; Pzu?—undifferentiated; Pzcc—metachert, argillite (Wagner et al., 1981). Fill patterns represent the distribution of bedrock units at the surface and not the underlying structure. “LGM” points to glacial extent during the last glacial maximum.

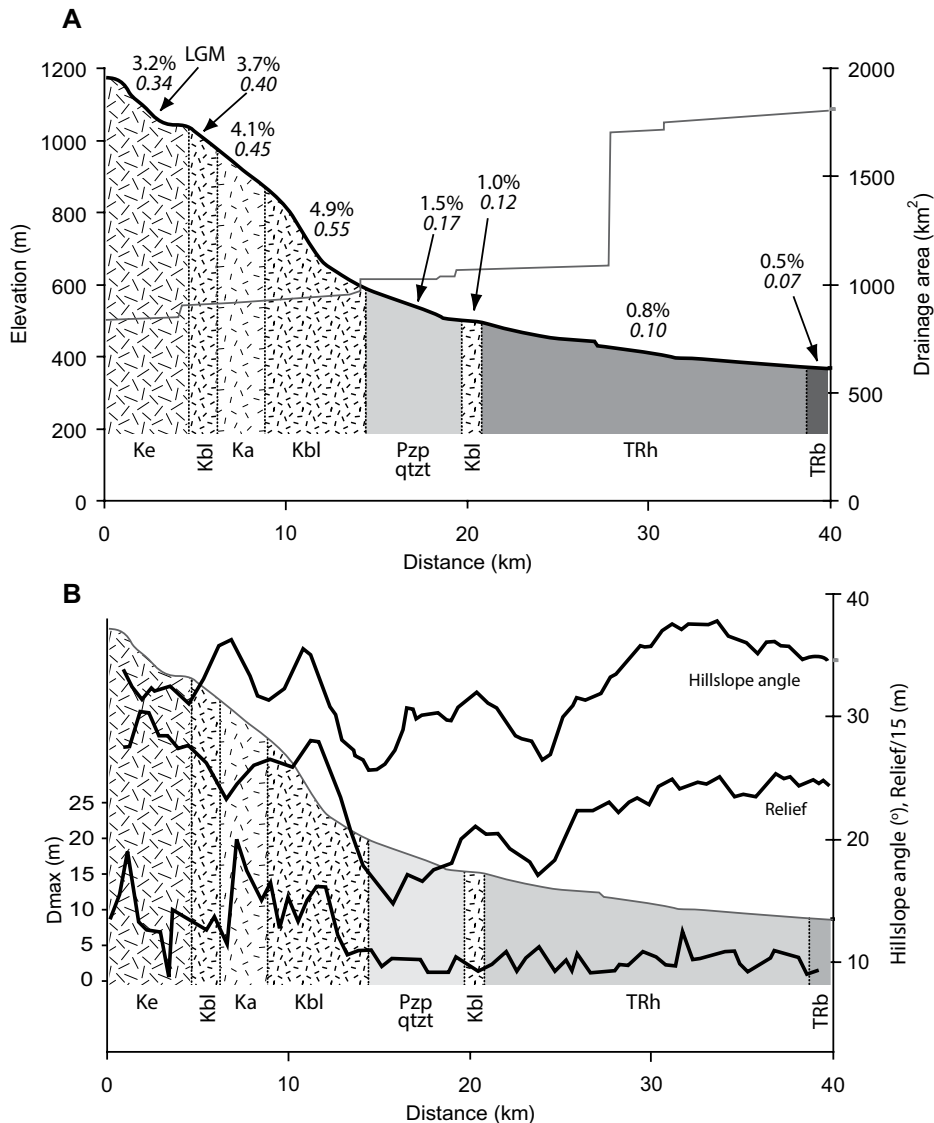
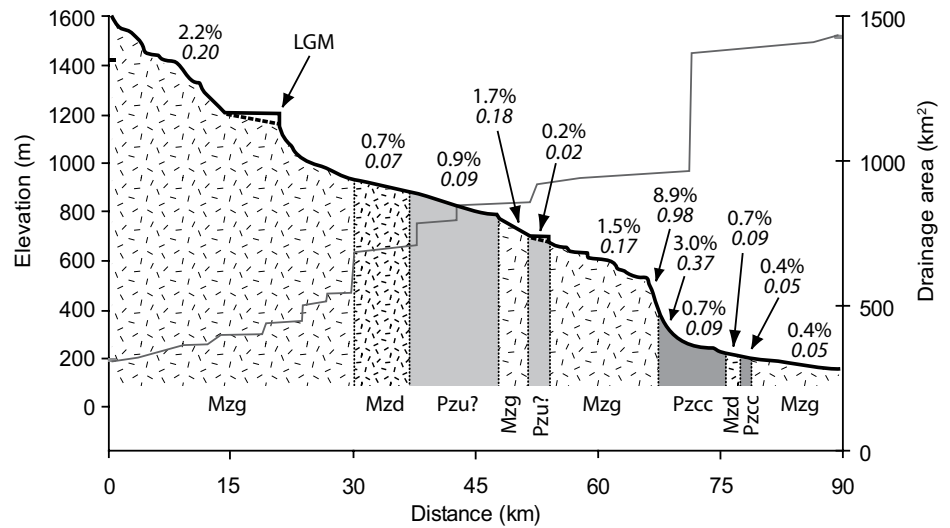


Figure 6. (A, B) Longitudinal profile, lithology, and other data along the Merced River. Gradient and k_s (steepness index; in *italics*) shown above each reach. Plutonic rocks designated by patterned fills; metasedimentary rocks designated by solid shading. Ke—coarse-grained granite, granodiorite; Kbl—medium-grained tonalite, granodiorite, quartz diorite; Ka—medium-grained granodiorite; Pzp qtzt—quartzite; TRh—phyllite, chert; TRb—phyllite (Bateman and Krauskopf, 1987; Peck, 2002). Fill patterns represent the distribution of bedrock units at the surface and not the underlying structure. “LGM” points to glacial extent during the last glacial maximum. D_{\max} —maximum particle size.

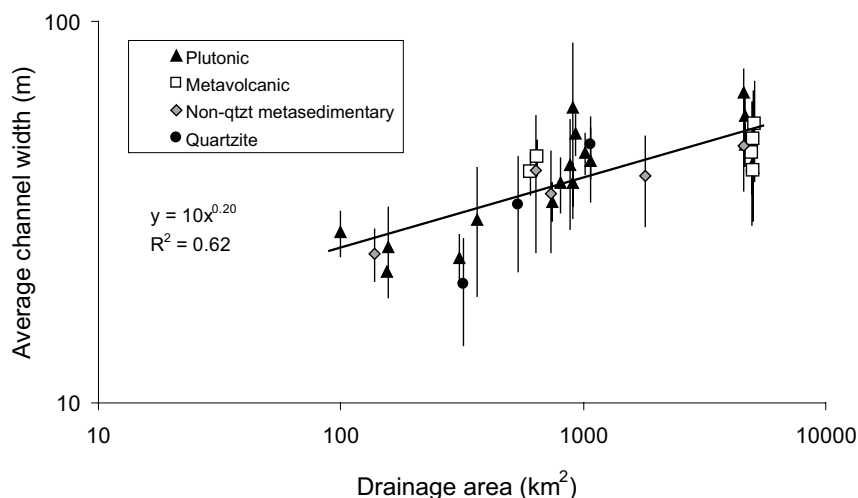


Figure 7. Reach-averaged channel widths increase with drainage area. The overlap of data from different rock types suggests that channel width is insensitive to lithology. The exponent on drainage area is lower than reported values from other regions (e.g., Lague, 2014), perhaps a result of the strong precipitation gradient driven by orographic effects (Mulch et al., 2006). Less precipitation at lower elevations would lead to lower discharges and channels narrower than might otherwise be expected given the drainage areas. Error bars = 1σ . non-qtzt—without quartzite.

TABLE 2. REACH-AVERAGED D_{MAX} (m) $\pm 1\sigma$ ACCORDING TO ROCK TYPE

| | Plutonic | Metavolcanic | Quartzite | Non-quartzite metasedimentary |
|--------------------------|--------------------|--------------------|--------------------|-------------------------------|
| North Fork Feather River | 5.7 ± 4.7 (34) | 5.3 ± 2.6 (24) | N.D. | 1.2 ± 0.7 (8) |
| South Yuba River | 4.7 ± 2.4 (65) | 2.9 ± 1.8 (13) | 3.2 ± 1.4 (25) | 2.7 ± 1.9 (49) |
| Merced River | 8.2 ± 4.8 (32) | N.D. | 2.2 ± 1.0 (13) | 2.5 ± 1.4 (28) |

Note: Sample sizes in parentheses. N.D.—no data; D_{MAX} (m)—maximum particle size.

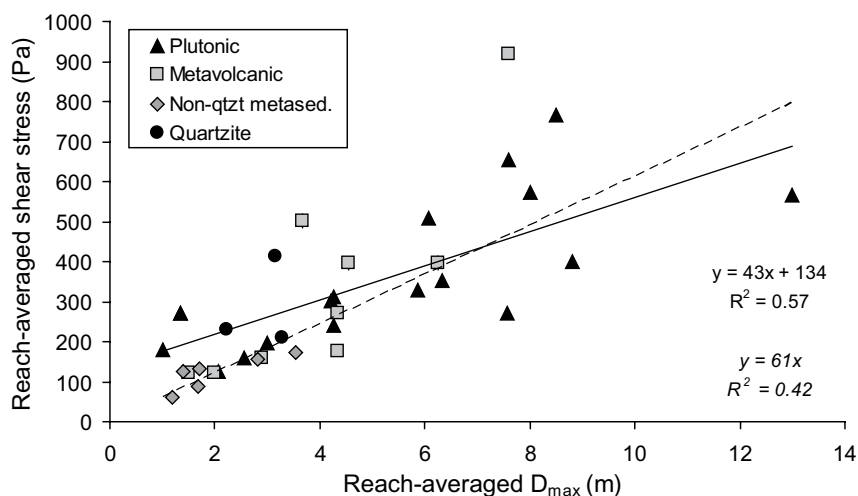


Figure 8. Shear stress increases with maximum boulder size. Regression for solid line is in regular font and regression for dashed line is in italics; both regressions are statistically significant ($p < 0.05$). Given the noise in the channel width data and the uncertainty in the discharge data, the strength of the correlation is surprising. A dimensionless shear stress for particle size D can be calculated with $\tau^* = \tau_b / ((\rho_s - \rho)gD)$, where ρ_s and ρ are the density of rock (2600 kg/m^3) and water, respectively (e.g., Lamb et al., 2015). Substituting the italicized regression into this equation yields 0.004 for τ^* , a value that is $\sim 10\times$ lower than the shear stress needed to move these large clasts. qtzt metased.—quartzite metasedimentary; D_{max} —maximum particle size.

There are no statistically significant differences in relief and average hillslope angle (typically ranging from $30\text{--}32^\circ$) between the plutonic, metavolcanic, and metasedimentary rocks. Nevertheless, particularly steep and deep canyons are associated with individual units. For example, two peaks in average hillslope angle are centered over narrow lithological units on the NF Feather River: metabasalt at km-29 and metagabbro at km-43 (Fig. 2B). These locally steep areas are associated with greater relief as well. The relationship between steep slopes, high relief, and individual lithological units finds its greatest expression along the South Yuba River, with peaks in these topographic metrics narrowly centered over units of granite (km-25), metachert (km-44), diorite (km-67), and quartz diorite (km-85) (Fig. 3B) (note that the gentle hillslopes near the headwaters of the South Yuba River reflect the low-relief topography of the Sierra Nevada uplands). A dip in hillslope angle, likely because of rock damage, is associated with a fault zone at km-40–41 along the South Yuba River (the other major dip, at km-34, is due to a junction with a large tributary). On the Merced River, peaks in hillslope angle and relief are centered over the Bass Lake tonalite (Kbl at km-11; Fig. 6B). Finally, relief and average hillslope angle were poorly correlated to channel gradient and k_s (data not shown); for example, the steepest hillslopes overlook the gentlest reach of the Merced River (km-30–40; Fig. 6A). The absence of a correlation between the river gradients and hillslope angles suggests that the valley walls are near their threshold slopes (except in the high-elevation, low-relief regions).

Reach Orientation and Lithology

There were 170 ~ 5 km reaches extracted from the metamorphic belts and 468 from the plutonic rocks. Longitudinal reaches dominate in the metamorphic rocks, indicating that their orientations are controlled by the NNW-SSE structural grain of the Sierra Nevada foothills (Fig. 10). In contrast, reaches flowing across plutonic bedrock are generally oriented down the slope of the range and, thus, their azimuths do not appear to be structurally controlled. The increased development of longitudinal channels in the metamorphic rocks is also apparent on regional geological maps (e.g., Wagner et al., 1991; Wagner et al., 1981) which show that many reaches in the metamorphic belts are parallel or subparallel to the structural grain and have 90° junction angles with other streams. In contrast, where these networks extend into plutonic rocks, they become dendritic.

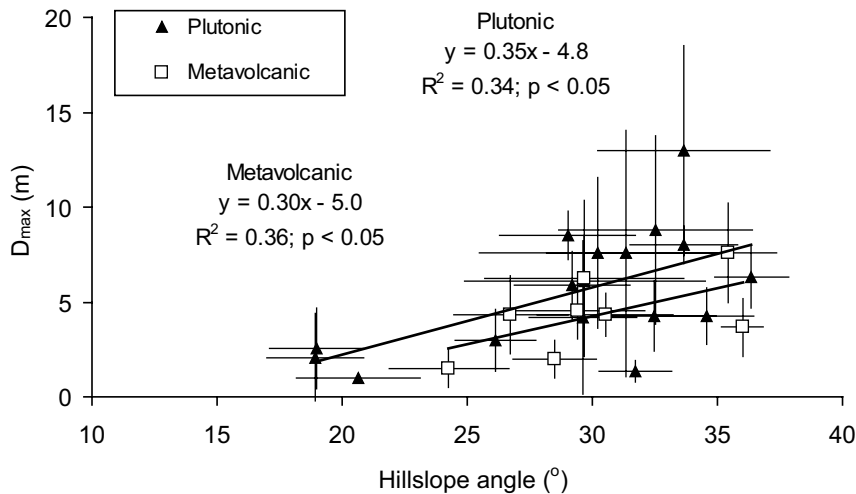


Figure 9. Maximum size of river boulders increases with hillslope angle in plutonic and metavolcanic bedrock. Both regressions are statistically significant. Error bars = 1σ .

DISCUSSION

River Gradient and Lithology

Along the five rivers analyzed here, changes in channel gradient are often associated with lithological transitions. The steepest reaches are typically in plutonic, metavolcanic, and quartzite bedrock while the gentlest reaches are generally underlain by non-quartzite metasedimentary bedrock (Table 1); Hack (1973) made similar observations in Appalachian streams. Indeed, for all five rivers analyzed, the median k_s values for the plutonic, metavolcanic, and quartzite rocks are about twice that of the non-quartzite metasedimentary rocks (Table 1). Also, for four of the five rivers, the highest median k_s value is in the plutonic rocks and the lowest is in the non-quartzite metasedimentary rocks. These consistent findings demonstrate that channel gradient is strongly influenced by lithology. If the steep reaches were due to actively migrating knickpoints, they would be randomly distributed across all of the lithologies.

There are exceptions to these general trends, however. For example, a reach of the NF Moke-lumne River flows over granite with the same gradient as the adjacent reach flowing over chert and argillite (km-80–90; Fig. 5), and, on the Merced River (km-20; Fig. 6A), a short reach underlain by granitic rock has a similar gentle gradient to the adjacent downstream reach flowing across phyllite and chert. This latter example is striking because the granitic bedrock lining this gentle reach also lines the steepest reach in the profile (km-15–20). The presence of these low-gradient granitic reaches at lower elevations suggest that they might have been exposed more often to subsurface water than their counterparts

at higher elevations and, therefore, the bedrock may have been weakened by chemical weathering (Callahan et al., 2019; Wahrhaftig, 1965).

In steady-state landscapes, where the uplift rate is matched by the incision rate, the gradients of bedrock rivers are typically assumed to be adjusted such that they are able to generate shear stresses sufficient to transport the supplied bedload and incise the bed (e.g., Lamb et al., 2015; Sklar and Dietrich, 2006a). In lithologically diverse terrain under steady-state conditions, therefore, the gradient of each reach will be adjusted to mobilize the sediment supplied to it from local and upstream sources, which may include different lithologies, and to incise the bedrock at a rate that matches the uplift rate (Duvall et al., 2004; Finnegan et al., 2017;

Hack, 1957; Hack, 1973). Thus, reaches underlain by resistant rock and/or supplied with large sediment will be steeper than those underlain by weak rock (e.g., Lecce, 1997).

The presence of high-elevation low-relief surfaces separated by knickpoints from high-relief regions at lower elevations and the absence of convincing evidence for sustained late Cenozoic uplift (Gabet, 2014 and references therein), however, indicate that the northern Sierra Nevada is not at steady-state. Nevertheless, reach gradient and resistance to fluvial erosion appear to be correlated in the actively incising portions of the landscape, and this correlation may be related to clast size. For example, the steep reach cut into quartz diorite at km-19 along the NF Feather River is associated with a 15-fold increase in the maximum sediment size relative to the gentler reach upstream cut into the same bedrock (km-10) (Fig. 2B). Similarly, along the South Yuba River, a positive relationship between the largest boulders and some of the steepest reaches can be seen at km-23–27 and km-70–76 (Fig. 3B).

The relationship between D_{\max} and estimated shear stresses during the 1997 flood (Fig. 8) suggests that the effect of lithology on gradient may be related to clast size via two processes. First, with the assumption that median particle size delivered from the local hillslopes scales with D_{\max} , the reaches may be adjusted to the caliber of the local sediment supply because incision cannot proceed until the bed is cleared of sediment (e.g., Lenzi et al., 2006). For example, at km-20 on the NF Feather River, the steep first kilometer of the reach underlain by monzonite may be a response to large boulders being delivered from the quartz diorite reach immediately upstream (Fig. 2B). In contrast, the second reach

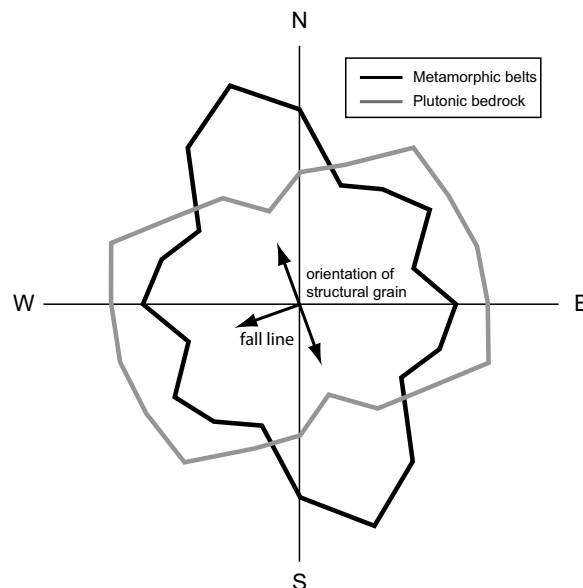


Figure 10. Rose diagram of azimuths of ~5-km reaches of river in the northern Sierra Nevada. Channel reaches flowing through metamorphic rocks in the foothills are dominantly aligned parallel to the structural grain and the range crest (i.e., approximately NNW-SSE). Reaches flowing across plutonic rocks are generally oriented down the slope of the range.

of monzonalite (km-30–38) is not preceded by a bedrock unit delivering large clasts and lacks a steep initial section. This observation suggests that the caliber of the sediment delivered by a particular lithology may be affecting the gradients of local reaches, as well as those farther downstream (Brocard and van der Beek, 2006; Duvall et al., 2004; Finnegan et al., 2017; Hack, 1957, 1973). Further evidence for the role of sediment supply on channel steepness may be seen at km-68 along the NF Mokelumne River (Fig. 11) where a very steep reach in granitic rock (8.9%) transitions to a reach in non-quartzite metasedimentary rock which is initially also steep (3.0%) but then grades into a much gentler slope (0.7%). The cliffs above the steep granitic reach are composed of exfoliation sheets which have few joints and, thus, break into large clasts as they fall into the river below. Some of these granitic boulders (albeit not the largest ones) are then likely transported downstream where they armor the relatively weak metasedimentary bedrock. Moreover, the failure of unjointed exfoliation sheets provides a strong negative feedback to river incision at this spot (Shobe et al., 2016).

As the channel cuts down, it removes the toe of the exposed sheet and triggers a slope failure which delivers 10–20 m boulders to the riverbed. At this point, incision is likely inhibited until these boulders are sufficiently comminuted that they can be cleared from the bed by fluvial transport processes; this process is likely so slow that the knickpoint is essentially stationary.

Whereas the role of local sediment supply appears to contribute to the lithological controls on reach gradient, this may only be a partial explanation. Indeed, many of the lithological contacts are associated with sharp breaks-in-slope. If the transport of material delivered from upstream reaches was consistently limiting local incision, then the breaks-in-slope at the lithological transitions would be more diffuse (e.g., km-68 on the NF Mokelumne River). Another process, then, that might link lithology, D_{\max} , and gradient is incision of the bed by the plucking of individual blocks. Because of differences in stress history and strength, different rock units will have different joint densities (Hancock and Engleider, 1989). Although joint spacing was not measured in this study, D_{\max} is assumed here to be a proxy for the maximum distance between joints (Hack, 1957), and the slope of an incising channel should increase with joint spacing where plucking dominates (Chatanantavet and Parker, 2009; Lamb et al., 2015). Indeed, differences in joint spacing could explain the significant differences in erodibility and gradient among the plutonic rocks. The effect of joint density could also explain the low gradients of reaches pass-

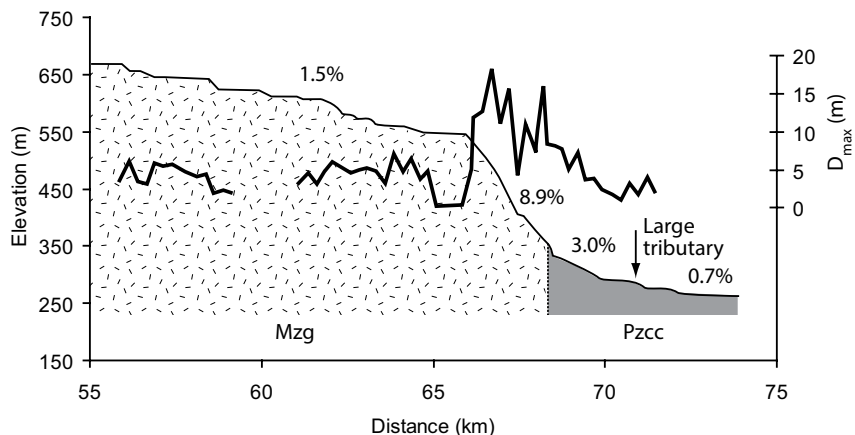


Figure 11. D_{\max} (maximum particle size) along a section of the North Fork Mokelumne River. The steep knickpoint in granite is associated with an abrupt increase in boulder size, a consequence of exfoliation sheets with low joint density lining the canyon walls. Large clasts delivered from these granitic slopes appear to be transported downstream to the reach in metasedimentary rock, resulting in an initially steep gradient in a bedrock unit that typically only supports gentle gradients and has D_{\max} values in the 2–4 m range. Gap in D_{\max} at ~60 km due to poor quality of the Google Earth imagery. Mzg—granitic; Pzcc—metasedimentary.

ing through fault zones where the fracturing of bedrock by tectonic activity may break the rock into pieces sufficiently small to be easily eroded by plucking (Molnar et al., 2007).

Whipple et al. (2000) estimated that incision by plucking in the Sierra Nevada was at least 10× faster than by abrasion, and a limited set observations in this study suggest that, indeed, abrasion does not appear to be a dominant process. Finer textures and higher quartz contents increase the tensile strength of crystalline rocks (Tuğrul and Zarif, 1999) and, thus, their resistance to abrasion (Sklar and Dietrich, 2001). Therefore, because the rate of abrasion increases with channel gradient (Johnson and Whipple, 2007; Lamb et al., 2008; Wohl and Ikeda, 1997), the slopes of individual reaches through plutonic rocks with different mineralogies should vary if abrasion is an important process. However, on the NF Feather River, alternating sequences of plutonic rocks with varying levels of quartz content (e.g., quartz diorite versus pyroxene diorite) or grain sizes (e.g., fine- to medium-grained pyroxene diorite versus coarse-grained monzonalite) do not lead to consistent differences in reach gradient (Fig. 2). Low abrasion rates may be related to the high tensile strengths of plutonic, metavolcanic, and quartzite bedrock that dominate the northern Sierra Nevada (Sklar and Dietrich, 2001). In addition, the presence of Eocene–Oligocene deposits throughout the region (Lindgren, 1911) attest to slow overall rates of erosion that might not yield a sufficient quantity of material to efficiently abrade the bed.

Finally, the role of time is important in the relationship between channel slope and lithology. Jansen et al. (2010) concluded that lithological controls on topography are more pronounced in post-orogenic landscapes because differential erosion has had more time to erode the weaker rocks and leave the stronger rocks behind; thus, differential erosion will amplify the topographic expression of variations in rock strength. For example, at the lower end of the NF Feather River profile (Fig. 2), a 100-m-high step has developed where a reach across a fault zone, which presumably weakened the rock, appears to have eroded faster than its upstream neighbors.

Drainage Patterns and Lithology

The reach-azimuth data (Fig. 10) and observations from the large-scale regional geological maps (Saucedo and Wagner, 1992; Strand, 1967; Wagner et al., 1991; Wagner et al., 1981) demonstrate that lithology has an important control on network structure in the northern Sierra Nevada. At the lower elevations, where the rivers are passing through the metamorphic belts, long reaches parallel to the structural grain are cut into weaker rock. Indeed, the strong bias for longitudinal valleys in the Sierra Nevada foothills misled early miners into concluding that gold-bearing gravels had been deposited by rivers with outlets to the north (Bateman and Wahrhaftig, 1966). Ninety-degree junction angles between trunk streams and their tributaries are also evidence for structural control on the spatial organization of the river networks (Howard, 1976).

In contrast, in the upper reaches of the watersheds where plutonic rocks dominate, the rivers are organized into dendritic networks. In the absence of any large-scale structural control, the rivers have a strong affinity for being oriented down the path of steepest descent (Fig. 10). Note, however, that these observations do not imply a complete lack of structural control on channels in the plutonic rocks. For example, the Merced River follows a large joint as it debouches from Yosemite Valley and, at the km-scale, there is a strong association between the orientations of fractures and streams (Ericson et al., 2005). Nevertheless, at the watershed-scale, there is little evidence for structural control on network configurations in the plutonic bedrock.

Implications for Interpreting the Geologic History of the Sierra Nevada

The age of the Sierra Nevada has been a contentious issue (e.g., Cassel et al., 2009; Gabet, 2014; Wakabayashi, 2013). While paleoelevation studies using stable isotopes have provided evidence that the Sierra Nevada has been a high range for much of the Cenozoic (Cassel et al., 2009; Crowley et al., 2008; Hren et al., 2010; Mix et al., 2016; Mulch et al., 2006; Poage and Chamberlain, 2002), others have relied on geomorphic analyses to argue that the range is much younger, having risen to its present heights only during the late Cenozoic (e.g., Jones et al., 2004; Lindgren, 1911; Wakabayashi, 2013; Yeend, 1974). The primary line of evidence used to support recent uplift is the difference in gradients of the remnants of Eocene and Oligocene paleochannels found throughout the northern half of the range. Lindgren (1911) linked these isolated deposits together to attempt to restore the course of the ancient rivers and noted that the reconstructed segments that flowed normal to the rangecrest (A and C in Fig. 12) were steeper than those flowing parallel to the rangecrest (B in Fig. 12). Lindgren concluded that the 0.7° difference in slopes was due to post-depositional westward-tilting and uplift of the northern Sierra. Since then, others have undertaken similar analyses of Lindgren's reconstructed channels and have also concluded that the Sierran block has been tilted by 0.7 – 1.0° in the late Cenozoic, resulting in significant uplift at the crest (Hudson, 1955; Jones et al., 2004; Yeend, 1974).

The validity of these analyses rests on several assumptions. First, they must assume that Lindgren's hypothetical reconstructions were accurate. However, some of Lindgren's paleochannels defy gravity and imply that water can flow uphill over high ridges (Gabet, 2014). This problem is highlighted in Hudson (1955), which applied a trigonometric analysis to "untilt" dif-

ferent sections of Lindgren's Tertiary Yuba River (Fig. 13) according to their azimuth to estimate the amount of late Cenozoic uplift. However, Hudson conceded that this approach "often produce(s) absurd results, such as negative gradients." Furthermore, Cassel et al. (2012b) and Durrell (1966) disproved two of Lindgren's paleochannel reconstructions by demonstrating that he had connected gravel patches that were receiving sediment from different source areas and, thus, could not have been part of the same river system. Second, studies that rely on Lindgren's paleochannels to investigate post-depositional tilt of the range must assume that these reconstructions represent contemporaneous rivers that were in steady-state. Cassel et al.

(2012a) and Cassel et al. (2012b) concluded, however, that gravel deposition progressed eastward up the range and that this general trend of aggradation was interrupted by periods of incision such that the isolated paleochannel remnants represent different generations of rivers. Finally, these studies assume that the Tertiary channels originally had smooth profiles such that any steps in the reconstructed profiles must be due to tilting (after accounting for reach orientation). This assumption, therefore, dismisses the role of lithology and structure in controlling channel gradient.

The analysis of the profiles of the modern rivers presented here can shed light on the relationship between gradient and orientation that has been used as evidence for recent tilting of the northern Sierra Nevada. For example, the range-parallel, low gradient segment in Lindgren's reconstruction of the ancient South Yuba River (B in Figs. 12 and 13) would have flowed across weak bedrock and a fault zone, conditions that yield low gradients in the modern South Yuba River. In contrast, the steep, range-normal segments in the putative ancient channel (A, C in Figs. 12 and 13) are in rock types that yield steep gradients in the modern rivers (i.e., plutonic, metavolcanic, and quartzite bedrocks). Assigning slopes for each lithological unit in segments A and C based on measurements from the modern rivers yields a difference in gradient of 1.3 – 1.9% (0.7 – 1.1°) between the range-parallel and range-normal segments (Fig. 13). In other words, lithology can account for 0.7 – 1.1° of the difference in the slopes of these segments whereas previous studies attributed this difference to uplift and tilting (Hudson, 1955; Jones et al., 2004; Lindgren, 1911; Yeend, 1974). Therefore, even if the first two assumptions were plausible, the dominant influence of lithology on river gradients cannot be dismissed when using the slopes of the paleochannels to infer uplift.

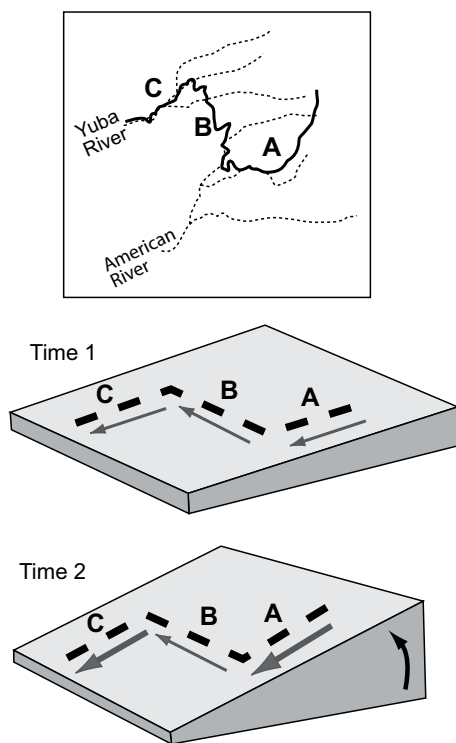


Figure 12. Hypothesis, proposed by others (Hudson, 1955; Jones et al., 2004; Lindgren, 1892; Yeend, 1974), explaining how the different gradients of paleochannel remnants support recent uplift of the Sierra Nevada. Map shows Lindgren's (1911) reconstruction of the ancient South Yuba River (solid line) superimposed over modern rivers (dotted lines). In the lower illustrations, dashed lines are the abandoned paleochannel remnants; arrow width represents relative gradients. At Time 1, the gradients of the transverse paleochannels (A, C) and the longitudinal reach (B) are similar. Hypothesized tilting and uplift (Time 2) increased the gradients of A and C but left the gradient of B unchanged.

Lithological versus Tectonic Knickpoints

Several studies have concluded that alleged significant tilting of the Sierra Nevada in the late Cenozoic created large knickpoints that quickly migrated up through the drainage networks and cut deep canyons (e.g., Clark et al., 2005; Figueroa and Knott, 2010; Matthes, 1930). For example, Wakabayashi (2013) proposed that an uplift-generated knickpoint swept up the American River system 3 m.y., incising to depths of 900 m. Similarly, Clark et al. (2005) analyzed knickpoints in tributaries to the Kern River, in the southern Sierra Nevada, and concluded that it had begun incising its canyon 3.5 m.y. as a result of contemporaneous uplift. Volcanic rocks older

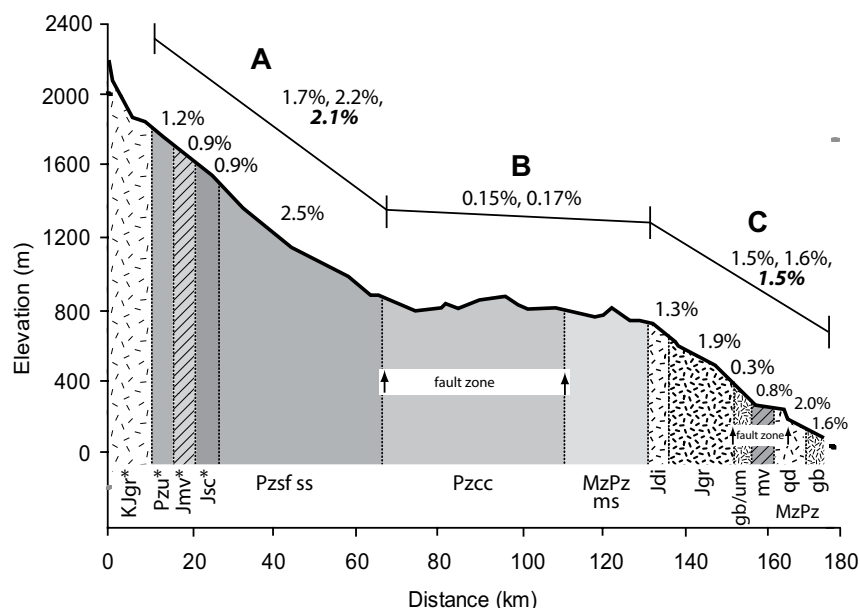


Figure 13. Profile of Lindgren's (1911) Tertiary Yuba River using data from Hudson (1955). The reconstructed profile, presented as a continuous feature, is based on isolated paleochannel remnants. Segments A, B, and C correspond to Figure 12; their gradients were calculated three different ways. The first value was calculated using each segment's distance as measured from the reconstructed profile and the second was calculated using each segment's "straight-line" distance to represent the regional slope; previous studies have attributed the differences in slopes between segments to tilting. The third value (in bold) is the distance-weighted average of the gradients of each lithological unit as determined from the modern South Yuba and South Fork American rivers (i.e., it is the slope of the segment that accounts for lithology). Since segment B would not have been tilted, no adjustment for lithology is needed for its gradient. Note the similarities in the slopes of the reconstructed channel and the slopes adjusted for lithology. Figures 3 and 4 present the bedrock unit descriptions and slopes. Fill patterns represent the distribution of bedrock units at the surface and not the underlying structure. Lithology in reaches with (*) inferred from surrounding outcrops because Cenozoic volcanic deposits cover the basement rock.

point was formed through differential erosion. Observations of the surrounding topography are particularly salient in the cases of knickpoints contained within a single unit, where there are no obvious lithological contrasts and a tectonic explanation would seem likely. For example, the knickpoint at km-11 on the Merced River is in the middle of a plutonic unit and, therefore, could be interpreted as a migrating knickpoint (Fig. 6B). If it were a migrating knickpoint, steep slopes and high relief would be expected immediately downstream of the feature (Hurst et al., 2013); instead, again, mean angle and relief drop to their lowest values. Tellingly, relative to the reach immediately downstream, D_{\max} increases 3-fold at the knickpoint face, suggesting an abrupt change in joint density. Indeed, Google Earth imagery confirms that the valley walls adjacent to the knickpoint are composed of large granitic sheets with few joints. Therefore, the rapid increase in channel slope, accompanied by peaks in hillslope angle, valley relief, and boulder size, most likely reflects a dip in joint density, rather than a migrating knickpoint.

CONCLUSION

The lithological heterogeneity of the northern Sierra Nevada provides an opportunity for exploring the lithological controls on river profiles and patterns. The channels studied here have steep reaches over lithologies generally considered to be resistant: plutonic, metavolcanic, and quartzite bedrock. Reaches with gentle gradients are generally found in weaker non-quartzite metasedimentary rock and across fault zones where rock damage is likely. Because of differences in erodibility, alternating sequences of weak and strong lithologies create river profiles with steps as high as ~600 m (e.g., the Merced and South Yuba rivers).

In addition to the river profiles, there is a strong lithological influence on the channel network patterns. In the metamorphic belts of the Sierra Nevada foothills, the river networks are trellis-like, with long reaches parallel to the structural grain. In the plutonic bedrock, the drainage networks are dendritic with most of the channel reaches oriented down the path of steepest descent.

Finally, the influence of rock type on river gradients and planforms demonstrates that caution should be used when using fluvial features to infer tectonic activity, particularly in lithologically complex terrain. In the northern Sierra Nevada, attempts to extract tilt information from paleochannels must account for the role of rock erodibility and structure in controlling channel steepness. Indeed, the different gradients of paleochannel remnants used to argue for

than the alleged uplift deep within the American and Kern canyons, however, refute these two studies (Gabet, 2014; Gabet et al., 2019) and highlight the importance of distinguishing migrating knickpoints generated by uplift from those forming in situ as a result of differential erosion (e.g., Cyr et al., 2014; Larue, 2008).

Multiple lines of evidence can be used to distinguish between tectonic and lithological knickpoints. For example, because uplift is a regional event, associated knickpoints ought to be found in similar topographic positions in neighboring drainages (Crosby and Whipple, 2006). In the Sierra Nevada, however, knickpoints are essentially randomly distributed with respect to topographic position, and knickpoints on adjacent streams typically do not project to a shared baselevel (Wahrhaftig, 1965). In addition, there are no strath terraces in the northern Sierra Nevada, another distinguishing characteristic

of migrating knickpoints, that could be used as evidence for the passage of knickpoints 100s of meters high (e.g., Crosby and Whipple, 2006). Because erosion rates in the northern Sierras are slow, as demonstrated by the presence of Eocene-age gravel deposits throughout the region (Lindgren, 1911), strath terraces formed 3 m.y. would have been preserved.

In addition to fluvial features, the surrounding topography can also be used to distinguish between tectonic and lithological knickpoints. A break-in-slope along the South Yuba River at km-25–35 might appear to be a migrating knickpoint sweeping up the river system (Fig. 3B); if this were the case, steep slopes and high relief would be expected immediately downstream of the feature because of the delay in hillslope response times (Hurst et al., 2013). Instead, mean angle and relief drop to their lowest values, suggesting that this knick-

late Cenozoic tilting and uplift of the northern Sierra Nevada can be wholly attributed to differences in lithology. Considering that the alleged tilt of paleochannels forms the foundation for the paradigm of late Cenozoic uplift of the northern Sierra Nevada and that the other lines of evidence are also disputed (Gabet, 2014), significant recent uplift of the region should be considered an unproven hypothesis.

ACKNOWLEDGMENTS

I am grateful to S. Mudd for his help in determining θ_{ref} and N. Finnegan and M. Lamb for their insights. I thank J. Jansen, E. Baynes, and an anonymous reviewer for their rigorous and stimulating comments.

REFERENCES CITED

- Bateman, P.C., and Krauskopf, K.B., 1987, Geologic map of the El Portal Quadrangle, west-central Sierra Nevada, California: U.S. Geological Survey, Miscellaneous Field Studies Map 1998, scale 1:62,500, <https://doi.org/10.3133/mf1998>.
- Bateman, P.C., and Wahrhaftig, C., 1966, Geology of the Sierra Nevada, in Bailey, E.H., ed., *Geology of Northern California*: California Division of Mines and Geology Bulletin 190, p. 107–172.
- Brocard, G.Y., and van der Beek, P.A., 2006, Influence of incision rate, rock strength, and bedload supply on bedrock river gradients and valley-flat widths: Field-based evidence and calibrations from western Alpine rivers (southeast France), in Willet, S.D., Hovius, N., Brandon, M.T., and Fisher, D.M., eds., *Penrose Conference Series: Tectonics, Climate, and Landscape Evolution*: Geological Society of America Special Paper 398, p. 101–126, [https://doi.org/10.1130/2006.2398\(07\)](https://doi.org/10.1130/2006.2398(07)).
- Brocklehurst, S.H., and Whipple, K.X., 2002, Glacial erosion and relief production in the Eastern Sierra Nevada, California: *Geomorphology*, v. 42, p. 1–24, [https://doi.org/10.1016/S0169-555X\(01\)00069-1](https://doi.org/10.1016/S0169-555X(01)00069-1).
- Callahan, R.P., Ferrier, K.L., Dixon, J., Dosseto, A., Hahn, W.J., Jessup, B.S., Miller, S.N., Hunsaker, C.T., Johnson, D.W., Sklar, L.S., and Riebe, C.S., 2019, Arrested development: Erosional equilibrium in the southern Sierra Nevada, California, maintained by feedbacks between channel incision and hillslope sediment production: *Geological Society of America Bulletin*, v. 131, no. 7–8, <https://doi.org/10.1130/B35006.1>.
- Cassel, E.J., Graham, S.A., and Chamberlain, C.P., 2009, Cenozoic tectonic and topographic evolution of the northern Sierra Nevada, California, through stable isotope paleoaltimetry in volcanic glass: *Geology*, v. 37, no. 6, p. 547–550, <https://doi.org/10.1130/G25572A.1>.
- Cassel, E.J., Graham, S.A., Chamberlain, C.P., and Henry, C.D., 2012a, Early Cenozoic topography, morphology, and tectonics of the northern Sierra Nevada and western Basin and Range: *Geosphere*, v. 8, no. 2, p. 229–249, <https://doi.org/10.1130/GES00671.1>.
- Cassel, E.J., Grove, M., and Graham, S.A., 2012b, Eocene drainage evolution and erosion of the Sierra Nevada batholith across northern California and Nevada: *American Journal of Science*, v. 312, p. 117–144, <https://doi.org/10.2475/02.2012.03>.
- Chatanantavet, P., and Parker, G., 2009, Physically based modeling of bedrock incision by abrasion, plucking, and macroabrasion: *Journal of Geophysical Research. Earth Surface*, v. 114, no. F4, <https://doi.org/10.1029/2008JF001044>.
- Clark, M.K., Maheo, G., Saleeby, J., and Farley, K.A., 2005, The non-equilibrium landscape of the southern Sierra Nevada, California: *GSA Today*, v. 15, no. 9, p. 4–10, [https://doi.org/10.1130/1052-5173\(2005\)015\[4:TNLOTS\]2.0.CO;2](https://doi.org/10.1130/1052-5173(2005)015[4:TNLOTS]2.0.CO;2).
- Crosby, B.T., and Whipple, K.X., 2006, Knickpoint initiation and distribution within fluvial networks: 236 waterfalls in the Waipoa River, North Island, New Zealand: *Geomorphology*, v. 82, no. 1, p. 16–38, <https://doi.org/10.1016/j.geomorph.2005.08.023>.
- Crowley, B.E., Koch, P.L., and Davis, E.B., 2008, Stable isotope constraints on the elevation history of the Sierra Nevada Mountains, California: *Geological Society of America Bulletin*, v. 120, p. 588–598, <https://doi.org/10.1130/B26254.1>.
- Cyr, A.J., Granger, D.E., Olivetti, V., and Molin, P., 2014, Distinguishing between tectonic and lithologic controls on bedrock channel longitudinal profiles using cosmogenic ^{10}Be erosion rates and channel steepness index: *Geomorphology*, v. 209, p. 27–38, <https://doi.org/10.1016/j.geomorph.2013.12.010>.
- Dühnforth, M., Anderson, R.S., Ward, D., and Stock, G.M., 2010, Bedrock fracture control of glacial erosion processes and rates: *Geology*, v. 38, no. 5, p. 423–426, <https://doi.org/10.1130/G30576.1>.
- Durrell, C., 1966, Tertiary and quaternary geology of the northern Sierra Nevada, in Bailey, E.H., ed., *Geology of Northern California*: California Division of Mines and Geology Bulletin 190, p. 185–197.
- Duvall, A.R., Kirby, E., and Burbank, D.W., 2004, Tectonic and lithologic controls on bedrock channel profiles and processes in coastal California: *Journal of Geophysical Research. Solid Earth*, v. 109, no. F3, <https://doi.org/10.1029/2003JF000086>.
- Ericson, K., Migon, P., and Olmo, M., 2005, Fractures and drainage in the granite mountainous area: A study from Sierra Nevada, USA: *Geomorphology*, v. 64, no. 1, p. 97–116.
- Fan, N., Chu, Z., Jiang, L., Hassan, M.A., Lamb, M.P., and Liu, X., 2018, Abrupt drainage basin reorganization following a Pleistocene river capture: *Nature Communications*, v. 9, no. 1, p. 3756, <https://doi.org/10.1038/s41467-018-06238-6>.
- Figueroa, A.M., and Knott, J.R., 2010, Tectonic geomorphology of the southern Sierra Nevada Mountains (California): Evidence for uplift and basin formation: *Geomorphology*, v. 123, p. 34–45, <https://doi.org/10.1016/j.geomorph.2010.06.009>.
- Finnegan, N.J., Klier, R.A., Johnstone, S., Pfeiffer, A.M., and Johnson, K., 2017, Field evidence for the control of grain size and sediment supply on steady-state bedrock river channel slopes in a tectonically active setting: *Earth Surface Processes and Landforms*, v. 42, p. 2338–2349, <https://doi.org/10.1002/esp.4187>.
- Fisher, G.B., Amos, C.B., Bookhagen, B., Burbank, D.W., and Godard, V., 2012, Channel widths, landslides, faults, and beyond: The new world order of high-spatial resolution Google Earth imagery in the study of earth surface processes, in Whitmeyer, S.J., Bailey, J. E., DePaor, D.G., and Ornduff, T., eds., *Google Earth and Virtual Visualizations in Geoscience Education and Research*: Geological Society of America Special Paper 492, p. 1–22, [https://doi.org/10.1130/2012.2492\(01\)](https://doi.org/10.1130/2012.2492(01)).
- Flint, J.J., 1974, Stream gradient as a function of order, magnitude, and discharge: *Water Resources Research*, v. 10, no. 5, p. 969–973, <https://doi.org/10.1029/WR010i005p0969>.
- Gabet, E.J., 2014, Late Cenozoic uplift of the Sierra Nevada, California? A critical analysis of the geomorphic evidence: *American Journal of Science*, v. 314, p. 1224–1257, <https://doi.org/10.2475/08.2014.03>.
- Gabet, E.J., Schaffer, J.P., Peppin, W.A., and Miggins, D.P., 2019, Corrigendum to Late Cenozoic uplift of the Sierra Nevada, California? A critical analysis of the geomorphic evidence: *American Journal of Science*, v. 319, no. 6, <https://doi.org/10.2475/06.2019.04>.
- Gillespie, A.R., and Clark, D.H., 2011, Glaciations of the Sierra Nevada, California, USA, in Ehlers, J., Gibbard, P.L., and Hughes, P. D., eds., *Quaternary Glaciations: Extent and Chronology: A Closer Look*: Amsterdam, The Netherlands, Elsevier, v. 15, p. 447–462, <https://doi.org/10.1016/B978-0-444-53447-7.00034-9>.
- Hack, J.T., 1957, Studies of longitudinal profiles in Virginia and Maryland: U.S. Geological Survey Professional Paper 294-B, p. 45–97, <https://doi.org/10.3133/pp294B>.
- Hack, J.T., 1973, Stream-profile analysis and stream-gradient index: *Journal of Research of the U.S. Geological Survey*, v. 1, no. 4, p. 421–429.
- Hancock, P.L., and Engelder, T., 1989, Neotectonic joints: *Geological Society of America Bulletin*, v. 101, no. 10, p. 1197–1208, [https://doi.org/10.1130/0016-7606\(1989\)101<1197:NJ>2.3.CO;2](https://doi.org/10.1130/0016-7606(1989)101<1197:NJ>2.3.CO;2).
- Hanks, T.C., and Webb, R.H., 2006, Effects of tributary debris on the longitudinal profile of the Colorado River in Grand Canyon: *Journal of Geophysical Research. Earth Surface*, v. 111, no. F2, <https://doi.org/10.1029/2004JF000257>.
- Hietanen, A., 1973, Geology of the Pulga and Bucks Lake quadrangles, Butte and Plumas counties, California: U.S. Geological Survey Professional Paper 731, scale 1:48,000, <https://doi.org/10.3133/pp731>.
- Howard, A.D., 1976, Drainage analysis in geological interpretation: A summation: *The American Association of Petroleum Geologists Bulletin*, v. 51, no. 11, p. 2246–2259.
- Hren, M.T., Pagani, M., Erwin, D.M., and Brandon, M.T., 2010, Biomarker reconstruction of the early Eocene paleotopography and paleoclimate of the northern Sierra Nevada: *Geology*, v. 38, no. 1, p. 7–10, <https://doi.org/10.1130/G30215.1>.
- Hudson, F.S., 1955, Measurement of the deformation of the Sierra Nevada, California, since middle Eocene: *Geological Society of America Bulletin*, v. 66, p. 835–870, [https://doi.org/10.1130/0016-7606\(1955\)66\[835:MOTDOT\]2.0.CO;2](https://doi.org/10.1130/0016-7606(1955)66[835:MOTDOT]2.0.CO;2).
- Hurst, M.D., Mudd, S.M., Attal, M., and Hilley, G.E., 2013, Hillslopes record the growth and decay of landscapes: *Science*, v. 341, p. 868–871, <https://doi.org/10.1126/science.1241791>.
- Inoue, K., 1992, Downstream change in grain size of river bed sediments and its geomorphological implications in the Kanto Plain, central Japan: *Geographical Review of Japan*, v. 65, no. 2, p. 75–89, <https://doi.org/10.4157/grj1984b.65.75>.
- Jansen, J.D., Codilean, A.T., Bishop, P., and Hoey, T.B., 2010, Scale dependence of lithological control on topography: Bedrock channel geometry and catchment morphometry in western Scotland: *The Journal of Geology*, v. 118, no. 3, p. 223–246, <https://doi.org/10.1086/651273>.
- Johnson, B.D., 2015, Lithologic controls on knickpoint formation in Sierra Nevada bedrock channels [M.S. thesis]: San Jose, California, USA, San José State University, 62 p., <https://doi.org/10.31979/etd.36vj-4qzk>.
- Johnson, J.P.L., and Whipple, K.X., 2007, Feedbacks between erosion and sediment transport in experimental bedrock channels: *Earth Surface Processes and Landforms*, v. 32, no. 7, p. 1048–1062, <https://doi.org/10.1002/esp.1471>.
- Jones, C.H., Farmer, G.L., and Unruh, J.R., 2004, Tectonics of Pliocene removal of lithosphere of the Sierra Nevada, California: *Geological Society of America Bulletin*, v. 116, no. 11–12, p. 1408–1422, <https://doi.org/10.1130/B25397.1>.
- Lague, D., 2014, The stream power river incision model: Evidence, theory and beyond: *Earth Surface Processes and Landforms*, v. 39, no. 1, p. 38–61, <https://doi.org/10.1002/esp.3462>.
- Lamb, M.P., Dietrich, W.E., and Sklar, L.S., 2008, A model for fluvial bedrock incision by impacting suspended and bed load sediment: *Journal of Geophysical Research. Earth Surface*, v. 113, no. F3, <https://doi.org/10.1029/2007JF000915>.
- Lamb, M.P., Finnegan, N.J., Scheingross, J.S., and Sklar, L.S., 2015, New insights into the mechanics of fluvial bedrock erosion through flume experiments and theory: *Geomorphology*, v. 244, p. 33–55, <https://doi.org/10.1016/j.geomorph.2015.03.003>, (corrigendum: <http://dx.doi.org/10.1016/j.geomorph.2018.05.028>).
- Larue, J.-P., 2008, Effects of tectonics and lithology on long profiles of 16 rivers of the south Central Massif border between the Aude and the Orb (France): *Geomorphology*, v. 93, p. 343–367, <https://doi.org/10.1016/j.geomorph.2007.03.003>.
- Lecce, S.A., 1997, Nonlinear downstream changes in stream power on Wisconsin's Blue River: *Annals of the Association of American Geographers*, v. 87, no. 3, p. 471–486, <https://doi.org/10.1111/1467-8306.00064>.
- Lenzi, M.A., Mao, L., and Comiti, F., 2006, When does bedload transport begin in steep boulder-bed streams?: *Hydrological Processes*, v. 20, no. 16, p. 3517–3533, <https://doi.org/10.1002/hyp.6168>.

- Lin, R.-G., and St. John, P., 2017, From extreme drought to record rain: Why California's drought-to-deluge cycle is getting worse: Los Angeles, California, USA, Los Angeles Times, <https://www.latimes.com/local/lanow/la-me-record-rains-20170410-story.html>.
- Lindgren, W., 1892, Two Neocene rivers of California: Geological Society of America Bulletin, v. 4, p. 257–298, <https://doi.org/10.1130/GSAB-4-257>.
- Lindgren, W., 1911, The Tertiary gravels of the Sierra Nevada of California: U.S. Geological Survey Professional Paper 73, 226 p., <https://doi.org/10.3133/pp73>.
- Ludington, S., Moring, B.C., Miller, R.J., Flynn, K.S., Stone, P.A., and Bedford, D.R., 2005, Preliminary integrated databases for the United States-western states: California, Nevada, Arizona, and Washington: U.S. Geological Survey Open File Report 2005-1305, <https://doi.org/10.3133/ofr20051305>.
- Matthes, F.E., 1930, Geologic history of the Yosemite Valley: U.S. Geological Survey Professional Paper 160, 137 p., <https://doi.org/10.3133/pp160>.
- Mix, H.T., Ibarra, D.E., Mulch, A., Graham, S.A., and Chamberlain, C.P., 2016, A hot and high Eocene Sierra Nevada: Geological Society of America Bulletin, v. 128, p. 531–542, <https://doi.org/10.1130/B31294.1>.
- Molnar, P., Anderson, R. S., and Anderson, S. P., 2007, Tectonics, fracturing of rock, and erosion: Journal of Geophysical Research. Earth Surface, v. 112, no. F3, <https://doi.org/10.1029/2005JF000433>.
- Montgomery, D.R., and Gran, K.B., 2001, Downstream variations in the width of bedrock channels: Water Resources Research, v. 37, no. 6, p. 1841–1846, <https://doi.org/10.1029/2000WR900393>.
- Mudd, S.M., Attal, M., Milodowski, D.T., Grieve, S.W., and Valters, D.A., 2014, A statistical framework to quantify spatial variation in channel gradients using the integral method of channel profile analysis: Journal of Geophysical Research. Earth Surface, v. 119, p. 138–152, <https://doi.org/10.1002/2013JF002981>.
- Mudd, S.M., Clubb, F.J., Gailleton, B., and Hurst, M.D., 2018a, How concave are river channels?: Earth Surface Dynamics, v. 6, p. 505–523, <https://doi.org/10.5194/esurf-6-505-2018>.
- Mudd, S.M., Clubb, F.J., Gailleton, B., Hurst, M.D., Milodowski, D.T., and Valters, D.A., 2018b, The LSDTopoTools Chi Mapping Package (Version 1.11): Zenodo, <https://doi.org/10.5281/zenodo.1291889>.
- Mulch, A., Graham, S.A., and Chamberlain, C.P., 2006, Hydrogen isotopes in Eocene river gravels and paleoelevation of the Sierra Nevada: Science, v. 313, p. 87–89, <https://doi.org/10.1126/science.1125986>.
- National Agricultural Imagery Program (NAIP), 2018, NAIP Imagery: U.S. Department of Agriculture Farm Service Agency, <https://www.fsa.usda.gov/programs-and-services/aerial-photography/imagery-programs/naip-imagery/>.
- O'Callaghan, J.F., and Mark, D.M., 1984, The extraction of drainage networks from digital elevation data: Computer Vision Graphics and Image Processing, v. 28, p. 323–344, [https://doi.org/10.1016/S0734-189X\(84\)80011-0](https://doi.org/10.1016/S0734-189X(84)80011-0).
- Parrish, J.G., 2006, Simplified geological map of California: California Geological Survey, scale 1:2,250,000, sheet 57.
- Pavano, F., Pazzaglia, F.J., and Catalano, S., 2016, Knick-points as geomorphic markers of active tectonics: A case study from northeastern Sicily (southern Italy): Lithosphere, v. 8, no. 6, p. 633–648, <https://doi.org/10.1130/L577.1>.
- Peck, D.L., 2002, Geologic map of the Yosemite quadrangle, central Sierra Nevada, California: U.S. Geological Survey, IMAP 2751, scale 1:62,500, 1 sheet, <https://doi.org/10.3133/i2751>.
- Perron, J.T., and Royden, L., 2013, An integral approach to bedrock river profile analysis: Earth Surface Processes and Landforms, v. 38, no. 6, p. 570–576, <https://doi.org/10.1002/esp.3302>.
- Phillips, J.D., and Lutz, J.D., 2008, Profile convexities in bedrock and alluvial streams: Geomorphology, v. 102, p. 554–566, <https://doi.org/10.1016/j.geomorph.2008.05.042>.
- Pike, A.S., Scatena, F.N., and Wohl, E.E., 2010, Lithological and fluvial controls on the geomorphology of tropical montane stream channels in Puerto Rico: Earth Surface Processes and Landforms, v. 35, p. 1402–1417, <https://doi.org/10.1002/esp.1978>.
- Poage, M.A., and Chamberlain, C.P., 2002, Stable isotopic evidence for a Pre-Middle Miocene rain shadow in the western Basin and Range: Implications for the paleotopography of the Sierra Nevada: Tectonics, v. 21, no. 4, p. 16–16–10.
- Saucedo, G.J., and Wagner, D.L., 1992, Geologic map of the Chico quadrangle, California: U.S. Geological Survey, California Division of Mines and Geology, Regional Geologic Map 7A, scale 1:250,000, https://ngmdb.usgs.gov/Prodesc/proddesc_63087.htm.
- Shobe, C.M., Tucker, G.E., and Anderson, R.S., 2016, Hill-slope-derived blocks retard river incision: Geophysical Research Letters, v. 43, no. 10, p. 5070–5078, <https://doi.org/10.1002/2016GL069262>.
- Sklar, L.S., and Dietrich, W.E., 2001, Sediment and rock strength controls on river incision into bedrock: Geology, v. 29, no. 12, p. 1087–1090, [https://doi.org/10.1130/0091-7613\(2001\)029<1087:SARSCO>2.0.CO;2](https://doi.org/10.1130/0091-7613(2001)029<1087:SARSCO>2.0.CO;2).
- Sklar, L.S., and Dietrich, W.E., 2006a, The role of sediment in controlling steady-state bedrock channel slope: Implications of the saltation-abrasion incision model: Geomorphology, v. 82, no. 1–2, p. 58–83, <https://doi.org/10.1016/j.geomorph.2005.08.019>.
- Sklar, L.S., and Dietrich, W.E., 2006b, The role of sediment in controlling steady-state bedrock channel slope: Implications of the saltation-abrasion incision model: Geomorphology, v. 82, no. 1–2, p. 58–83, <https://doi.org/10.1016/j.geomorph.2005.08.019>.
- Snow, C.A., and Scherer, H., 2006, Terranes of the western Sierra Nevada foothills metamorphic belt, California: A critical review: International Geology Review, v. 48, no. 1, p. 46–62, <https://doi.org/10.2747/0020-6814.48.1.46>.
- Snyder, N.P., Whipple, K.X., Tucker, G.E., and Merritts, D.J., 2003, Importance of a stochastic distribution of floods and erosion thresholds in the bedrock river incision problem: Journal of Geophysical Research. Solid Earth, v. 108, no. B2, p. 1–14, <https://doi.org/10.1029/2001JB001655>.
- Strand, R.G., 1967, Geologic map of California, Mariposa sheet: U.S. Geological Survey, California Division of Mines and Geology, scale 1:250,000, https://ngmdb.usgs.gov/Prodesc/proddesc_491.htm.
- Tuğrul, A., and Zarif, I.H., 1999, The correlation of mineralogical and textural characteristics with engineering properties of selected granitic rocks from Turkey: Engineering Geology, v. 51, p. 303–317, [https://doi.org/10.1016/S0013-7952\(98\)00071-4](https://doi.org/10.1016/S0013-7952(98)00071-4).
- U.S. Army Corps of Engineers (USACE), 1994, Hydraulic Design of Flood Control Channels: Washington, D.C., U.S. Army Corps of Engineers, 183 p.
- Wagner, D.L., Jennings, C.W., Bedrossian, T.L., and Bortugno, E.J., 1981, Geologic map of the Sacramento quadrangle, California: U.S. Geological Survey, California Division of Mines and Geology, Regional Geologic Map 1A, scale 1:250,000, https://ngmdb.usgs.gov/Prodesc/proddesc_520.htm.
- Wagner, D.L., Bortugno, E.J., and McJunkin, R.D., 1991, Geological map of the San Francisco-San Jose quadrangle, California: U.S. Geological Survey, California Division of Mines and Geology, Regional Geologic Map 5A, scale 1:250,000, https://ngmdb.usgs.gov/Prodesc/proddesc_519.htm.
- Wahrhaftig, C., 1965, Stepped topography of the southern Sierra Nevada, California: Geological Society of America Bulletin, v. 76, p. 1165–1190, [https://doi.org/10.1130/0016-7606\(1965\)76\[1165:STOTSS\]2.0.CO;2](https://doi.org/10.1130/0016-7606(1965)76[1165:STOTSS]2.0.CO;2).
- Wakabayashi, J., 2013, Paleochannels, stream incision, erosion, topographic evolution, and alternative explanations of paleoaltimetry, Sierra Nevada, California: Geosphere, v. 9, no. 2, p. 191–215, <https://doi.org/10.1130/GES00814.1>.
- Whipple, K.X., Hancock, G.S., and Anderson, R.S., 2000, River incision into bedrock: Mechanics and relative efficacy of plucking, abrasion, and cavitation: Geological Society of America Bulletin, v. 112, no. 3, p. 490–503, [https://doi.org/10.1130/0016-7606\(2000\)112<490:RIIBMA>2.0.CO;2](https://doi.org/10.1130/0016-7606(2000)112<490:RIIBMA>2.0.CO;2).
- Wobus, C.W., Whipple, K.X., Kirby, E., Snyder, N., Johnson, J., Spyropolou, K., Crosby, B.T., and Sheehan, D., 2006, Tectonics from topography: Procedures, promises, and pitfalls: Geological Society of America Bulletin, v. 398, p. 55–74.
- Wohl, E.E., and Ikeda, H., 1997, Experimental simulation of channel incision into a cohesive substrate at varying gradients: Geology, v. 25, no. 4, p. 295–298, [https://doi.org/10.1130/0091-7613\(1997\)025<0295:ESOCII>2.3.CO;2](https://doi.org/10.1130/0091-7613(1997)025<0295:ESOCII>2.3.CO;2).
- Yeend, W. E., 1974, Gold-bearing gravel of the ancestral Yuba River, Sierra Nevada, California: U.S.G.S Professional Paper 772, p. 1–44.
- Zimmer, P.D., and Gabet, E.J., 2018, Assessing glacial modification of bedrock valleys using a novel approach: Geomorphology, v. 318, p. 336–347, <https://doi.org/10.1016/j.geomorph.2018.06.021>.

SCIENCE EDITOR: ROB STRACHAN
ASSOCIATE EDITOR: JOHN JANSEN

MANUSCRIPT RECEIVED 31 AUGUST 2018
REVISED MANUSCRIPT RECEIVED 5 APRIL 2019
MANUSCRIPT ACCEPTED 28 MAY 2019

Printed in the USA